IEEE Access
Multidisciplinary ⋮ Rapid Review ⋮ Open Access Journal

Received 3 November 2023, accepted 15 November 2023, date of publication 20 November 2023,
date of current version 28 November 2023.

Digital Object Identifier 10.1109/ACCESS.2023.3335121

RESEARCH ARTICLE

The Application of a Sliding Mode Observer in a Speed Sensor Fault Tolerant PMSM Drive System

KAMILA JANKOWSKA[1], VIKTOR PETRO[2], MATEUSZ DYBKOWSKI[1], AND KAROL KYSLAN[2], (Member, IEEE)
[1]Department of Electrical Machines, Drives and Measurements, Wrocław University of Science and Technology, 50-370 Wrocław, Poland
[2]Department of Electrical Engineering and Mechatronics, Technical University of Košice, 042 00 Košice, Slovakia

Corresponding author: Karol Kyslan (karol.kyslan@tuke.sk)

This work was supported by the Scientific Grant Agency of the Ministry of Education, Science, Research and Sport of the Slovak Republic and Slovak Academy of Sciences (VEGA) under the project VEGA 1/0363/23.

ABSTRACT The fault-tolerant control system (FTCS) for a permanent magnet synchronous motor (PMSM) is presented and an analysis of speed sensor faults is proposed in this paper. The detection and compensation of speed sensor faults is based on the simple comparison of the measured signals with the signals estimated by reduced-order sliding mode observer (SMO). The focus of the work is on the presentation of simulation and experimental research for the most common speed sensor failure types: complete signal loss, gain error, and measurement noise. Additionally, an analysis of different operating conditions of the PMSM drive system is presented, which highlights the system's behaviour under various conditions. The presented algorithm enables the fast detection and compensation of failures with very short detection times, making it a versatile solution for a PMSM drive system and improving its overall reliability.

INDEX TERMS Fault tolerant control, permanent magnet synchronous machine, sensor fault, sliding mode observer.

I. INTRODUCTION

Permanent magnet synchronous motors (PMSMs) are often used in advanced applications that require an increased level of safety. An example of such applications can be electromobility or aircraft. Failure in these types of control systems can lead to a disaster. Therefore, Fault-Tolerant Control (FTC) systems are used there [1]. The task of such systems is real-time monitoring and diagnostics. Once a failure has occurred, it should not only be detected but also located and compensated for. The adoption of such systems guarantees not only reliable operation under normal circumstances but also resilience following the occurrence of a failure.

As per existing literature, Fault-Tolerant Control (FTC) systems can be categorized into two primary groups [2], [3], [4]. The first of them is passive systems (PFTC), where controllers are used to compensate for the impact of damage on the control structure, e.g. controllers based on fuzzy logic or a neural network. However, a drawback of such a system is its inability to detect damage; it solely focuses on counteracting its influence which means that the failure may still proceed. In contrast, the second category, active systems (AFTC), represents a more advanced approach. AFTC contain blocks responsible for damage detection and systems to their compensate for them. Compensation can take place at the hardware level, e.g. through additional sensors or software, where the damaged element is replaced with an appropriate algorithm. Compared to PFTCs, AFTCs require much more computing resources [5].

Drive systems with PMSMs are primarily exposed to three main types of faults: damage to the motor, damage to the frequency converter, and damage to the measuring sensors [6]. In the case of damage to the motor itself, it is difficult to apply failure compensation and the system should be turned off as soon as possible. Within this scenario, existing literature predominantly focuses on the detection of failures. An example of failure compensation is shown

The associate editor coordinating the review of this manuscript and approving it for publication was Jinquan Xu.

in [7], wherein supplementary windings are employed to address short-circuit failures in the stator windings. In a failure occurring within frequency converter, the potential for failure compensation increases. However, compensation typically relies on hardware redundancy. Both preceding failure scenarios are identified through the utilization of measuring sensors, constituting the third primary category of failures [8], [9].

For the purpose of achieving high-quality control, a drive system with PMSM should be equipped with a speed/position sensor, a minimum of two current sensors, and a DC link voltage sensor [10]. The most important of these is the speed sensor. To this end, resolvers and encoders are the most frequently employed solutions. Speed sensors, however, are susceptible to various forms of damage. Four main categories can be distinguished [11]:

(a) complete loss of the signal or its interruption,
(b) maintaining a constant value for speed even if the motor shaft moves with different speeds,
(c) variable gain change, where the measured signal is reduced or amplified compared to its real value,
(d) distortions of the measured signal with a noise, bias, or shift.

Speed sensor failures may concern mechanical, electrical, or optical parts. The PMSM drive operates in a way that requires accurate knowledge of the rotor angle to function correctly. In the majority of PMSM drives, the mechanical speed is calculated using the same encoder that measures the mechanical angle. In contrast to drives with induction motors, the malfunction of the speed sensor has more serious consequences and requires a swift and highly responsive detection and compensation mechanism. A short-term loss of measurement leads to the loss of system stability and shutdown of its operation by safety systems. The detection time is of utmost importance. For this reason, a lot of works related to the detection of speed transducer faults presents only simulation results [12], [13].

The work [14] described the use of a sliding mode observer (SMO) in a system that tolerates damage to the speed sensor. The study focused on a specific failure type: the complete loss of the measured signal. When this failure arises, the SMO was used to estimate information regarding the position of the motor shaft. The simulation results were presented only for medium and high-speed regions. Tests were also carried out without motor being loaded.

A more extensive solution was presented in [15]. The SMO was utilized for the generation of residual signals for the detection of both current and speed sensors. A comparison of the estimated and measured values of both current and speed was used for failure detection. The authors considered a constant fault and a noise fault. The research involves simulation tests only and the study does not address the failure detection times.

The Luenberger observer (LO) was used for speed estimation in [16]. Obtained signal was processed by wavelet transform. Employing this signal processing technique proposed solution aimed to enhance the immunity of the system to false alarms in failure detection. However, it also added complexity to the solution. Failure detection time was in the range of 0.1 to 1 s. Under experimental conditions it could lead to a loss of control system stability. Detection time increased with increasing speed. The solution proposed in [16] presented no experimental results and it was also shown that the use of additional signal processing methods extends the detection time.

The detection of the gain error was presented in [17]. The unknown input observer (UIO) was used to estimate the speed. The lowest detection time was 0.1 s, considerably depending on the motor speed value.

Other examples focus on the switchover between PI controller and fuzzy logic-based controller. In these systems, the extended Kalman filter (EKF) [18] or model reference adaptive system (MRAS) [19] was used for speed estimation.

The literature also presents solutions based on multiple observers [13], [20]. Their major disadvantages are the complexity of the system and high dependence on motor parameters [21].

The primary drawback of most of the works mentioned is the absence of the experimental results. A comparator that solely relies on comparing estimated speed and measured speed exhibits an unacceptably long detection time. When switching from measured to estimated speed, if detection time is too long, it will cause the loss of control stability. Hence, we will provide results with the examination of the detection time and propose a viable solution to address this issue.

An additional advantage of the solution proposed in this paper is the ability to detect all types of damages mentioned by other authors (usually only one or two types of damage is considered). In addition, the proposed solution manages to detect various types of failures based on raw signals, without any processing methods employed. Finally, the last element that distinguishes this paper from the literature is the presentation of results in a wide range of speeds, taking into account also dynamic states.

The article presents a thorough analysis of the operation of the system in various operating conditions of the drive. The speed sensor damage detection and compensation based on SMO and the q-axis current value in the rotor system are presented. Utilizing a current comparator enables faster detection compared to relying solely on the measured and estimated speed values. As a result, the work presents both simulation and experimental studies. The experimental results are the highlight of the article. Furthermore, the paper presents the detection of failures with high efficiency. The results show the operation at different values of speed and with the motor being loaded. Furthermore, the average detection times are listed.

The article is organized as follows. The initial section offers a literature review covering FTC systems and speed sensor fault detection techniques. The second chapter describes the theoretical foundations of the SMO used in the

fault tolerant drive setup. The third chapter describes the fault detection method and the control framework of the PMSM drive system. Chapters 4 to 5 present the simulation and experimental results of the tested failure detector. The last chapter contains a summary of the obtained findings.

II. THEORETICAL BACKGROUND OF SLIDING MODE OBSERVER FOR SPEED ESTIMATION

In this article, a SMO in the two-phase $\alpha\beta$ stator reference frame will be used. The state equation of the surface-mounted PMSM currents is defined as follows:

$$\begin{bmatrix} \dot{i}_\alpha \\ \dot{i}_\beta \end{bmatrix} = \frac{1}{L_s}\begin{bmatrix} -R_s & 0 \\ 0 & -R_s \end{bmatrix}\begin{bmatrix} i_\alpha \\ i_\beta \end{bmatrix} + \frac{1}{L_s}\begin{bmatrix} u_\alpha - e_\alpha \\ u_\beta - e_\beta \end{bmatrix}, \quad (1)$$

where i_α, i_β and u_α, u_β are stator currents in [A] and voltages in [V], respectively; e_α, e_β are back-EMF voltages components in [V], and R_s, L_s are stator phase resistance in [Ω] and inductance in [H], respectively. The back-EMF voltage components are expressed as:

$$\begin{aligned} e_\alpha &= -\omega_e \lambda_{PM} \sin(\theta_e), \\ e_\beta &= \omega_e \lambda_{PM} \cos(\theta_e), \end{aligned} \quad (2)$$

where ω_e is the electrical angular velocity in [rad/s], θ_e is the electrical rotor position in [rad], and λ_{PM} can be calculated from:

$$\lambda_{PM} = \frac{2k_t}{3p} = \frac{k_e}{p}, \quad (3)$$

where k_t is the torque constant in [Nm/A], k_e is the back-EMF constant [V/krpm] and p is the number of motor pole pairs.

The electrical rotor position and velocity are used for calculation of back-EMF voltage components as shown in (2)-(3). Conversely, the electrical position and speed can be obtained from (2)–(3) if the back-EMF voltage is high enough to be reliably estimated. This is the case for medium and high-speed drives, above 5-10% of nominal drive speed. The e_α and e_β components of the back-EMF voltage are estimated with an observer. The sliding mode observer (SMO) is among the most used algorithms due to its simple structure, low sensitivity to parameter variation, low computational requirements and high insensitivity to disturbances [22]. The reduced order SMO for back-EMF estimation is defined as follows:

$$\begin{bmatrix} \dot{\hat{i}}_\alpha \\ \dot{\hat{i}}_\beta \end{bmatrix} = \frac{1}{L_s}\begin{bmatrix} -R_s & 0 \\ 0 & -R_s \end{bmatrix}\begin{bmatrix} \hat{i}_\alpha \\ \hat{i}_\beta \end{bmatrix} + \frac{1}{L_s}\begin{bmatrix} u_\alpha - \hat{e}_\alpha - z_\alpha \\ u_\beta - \hat{e}_\beta - z_\beta \end{bmatrix}, \quad (4)$$

where superscript$\hat{}$indicates the estimated value. Values z_α, z_β in [V] are feedback signals of SMO. The task for the observer is to match measured stator currents i_α, i_β and observed stator currents $\hat{i}_\alpha, \hat{i}_\beta$. The observation errors are defined as:

$$s(x) = \begin{bmatrix} \bar{i}_\alpha \\ \bar{i}_\beta \end{bmatrix} = \begin{bmatrix} \hat{i}_\alpha - i_\alpha \\ \hat{i}_\beta - i_\beta \end{bmatrix}, \quad (5)$$

where $\bar{i}_\alpha$,$\bar{i}_\beta$ are the errors in [A] between the measured and the observed currents. The switching action occurs when:

$$s(x) = 0. \quad (6)$$

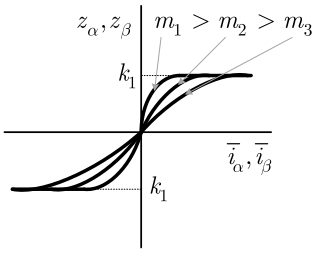

FIGURE 1. Shaping parameter of a hyperbolic function.

Equation (6) gives the switching surface $s(x)$ for the SMO. It represents the phase plane divided into two sections in which observation errors defined in (5) have different signs. The current observation errors are used as the input for the switching function. In the early stages of the SMO, a discontinuous sign function was commonly used [22]. However, utilizing sign function only introduces some level of noise and chattering to the output values. Recent solutions use continuous functions such as the limit, sigmoid or hyperbolic function [23], [24], [25]. In this article, a hyperbolic function is used:

$$\begin{bmatrix} z_\alpha \\ z_\beta \end{bmatrix} = k_1 \begin{bmatrix} \dfrac{e^{m\bar{i}_\alpha} - e^{-m\bar{i}_\alpha}}{e^{m\bar{i}_\alpha} + e^{-m\bar{i}_\alpha}} \\ \dfrac{e^{m\bar{i}_\beta} - e^{-m\bar{i}_\beta}}{e^{m\bar{i}_\beta} + e^{-m\bar{i}_\beta}} \end{bmatrix}, \quad (7)$$

where k_1 is the feedback gain and m is the shaping parameter. The function of the shaping parameter can is explained from Fig. 1.

The value of k_1 plays an important role in the observer's stability and performance. A proper Lyapunov function candidate is required to prove the convergence of the SMO. The description of the Lyapunov function can be found in [26]. To ensure the stability of the observer, the following condition must stand for the feedback gain value k_1:

$$k_1 > \max(|e_\alpha|, |e_\beta|). \quad (8)$$

The short time interval average values of the feedback signal components (7) represent the back-EMF components. To obtain these values a low-pass filter (LPF) can be used:

$$\begin{bmatrix} \hat{e}_\alpha \\ \hat{e}_\beta \end{bmatrix} = \frac{\omega_c}{s + \omega_c}\begin{bmatrix} z_\alpha \\ z_\beta \end{bmatrix}, \quad (9)$$

where ω_c is the cutoff frequency of LPS in [rad/s] usually selected according to the fundamental frequency of the stator current [27]. Rearranging (2), the estimated electrical rotor position can be calculated with actangent function:

$$\hat{\theta}_e = -\arctan\left(\frac{\hat{e}_\alpha}{\hat{e}_\beta}\right). \quad (10)$$

Note that (10) presents the operation of division of estimated back-EMF voltages which have a high content of harmonic components. The effect of noise and harmonics

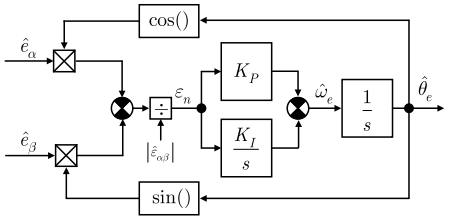

FIGURE 2. Quadrature PLL for speed and position estimation from the back EMF voltages.

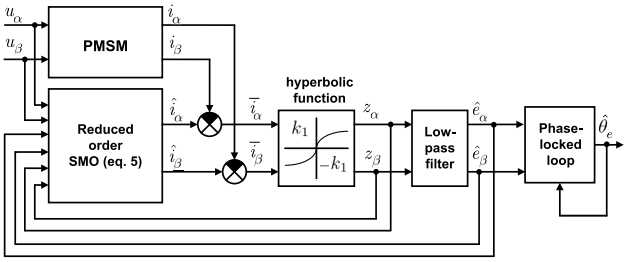

FIGURE 3. A block diagram of the reduced order SMO used for position and speed estimation.

can be mitigated utilizing phase-locked loop (PLL) [28], quadrature phase-locked loop (QPLL) [29] or second-order generalized integrator phase-locked loop (SOGI-PLL) [30]. The QPLL-type, as shown in Fig. 2, is used in this paper. The normalization signal is expressed as:

$$|e_{\alpha\beta}| = \sqrt{\hat{e}_\alpha^2 + \hat{e}_\beta^2}. \tag{11}$$

The response of QPLL estimator is independent of machine speed variation, what favors the QPLL over conventional PLL. The block diagram of the SMO including PLL is shown in Fig. 3.

The back-EMF values are not included as state values but they are considered to be disturbances whose values are obtained indirectly by matching of estimated and measured currents. The advantage of this approach is the reduced order of the observer and thus a lower computational burden comparing to higher order sliding mode observers. The SMO given by (1)–(9) is is referred to in the literature as reduced order observer or indirect observer [27], [31]. It will be used as a basis for our detection algorithm proposed and explained in the next section.

III. CONTROL STRUCTURE WITH A FAULT DETECTOR

The field-oriented control (FOC) structure was used in both simulation and experimental studies. It is a commonly used method of motor control that requires a speed sensor and current sensors for proper operation. Detection is based on the value of both measured and SMO-estimated q axis current and both measured and SMO-estimated speed. The estimated current $\hat{i}_q$ was obtained by applying Park transformation with the estimated value of electrical position $\hat{\theta}_e$. The value of $\hat{i}_q$ was used for detection because for some types of faults, the

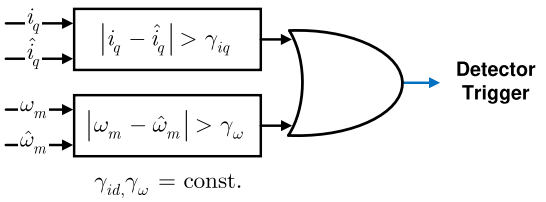

FIGURE 4. Working principle of a detection block based on signal comparation.

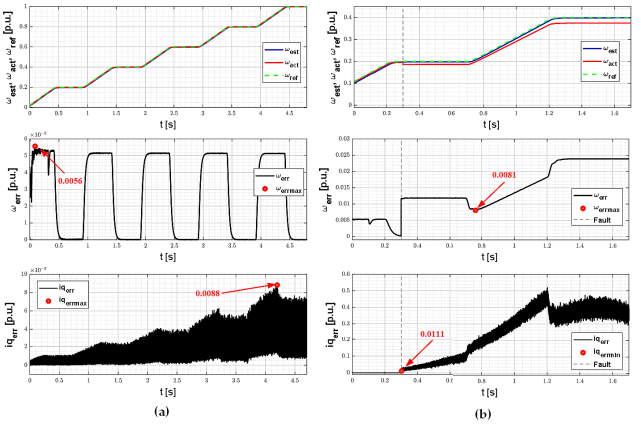

FIGURE 5. Example of transients of speed, speed error and current error under non-damage conditions (a) and under gain error (b) necessary for determination of threshold values.

current error symptoms appear earlier than speed error. If the differences between measured and estimated currents and speeds exceed a certain constant value, the detection block output is set to 1, and the control of the drive is switched to the sensorless mode. The working principle of the detection block is shown in Fig. 4.

The important part of the detection algorithm is the appropriate selection of thresholds that activate the sensorless mode. To find the most universal method possible, the solution obtained by simulation in different operating state will be given below in per-unit system. Threshold values of the switching sensorless mode can be determined in following steps:

1) Firstly, the speed and current error values in the full speed range with loaded machine has to be obtained in the undamaged state. A random increase in error values may occur during those transients. Initial values resulting from the poor operation properties of the SMO at the low speeds (< 0.05 ω_{ref}) have to be rejected.
2) The maximum value of the error during the no-damage state has to be found. The purpose of this step is to eliminate false alarms about damage. This is the upper boundary.
3) Then, waveforms of the speed and current errors for a damage type that has only a marginal impact on the control structure have to be obtained. A gain error of 0.95 ω_{ref} was chosen in this step as a damage.

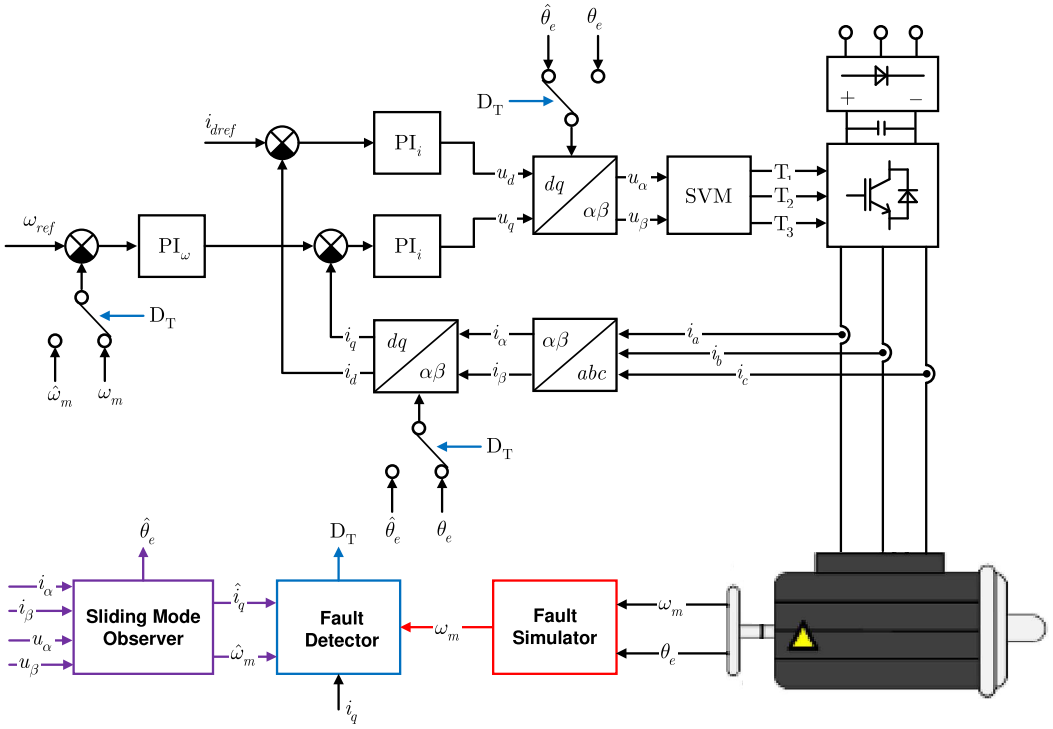

FIGURE 6. Overall control structure with the fault simulation and detection block.

4) After enabling the fault, the minimum value of speed and current errors has to be obtained. The purpose of this step is to find the lowest possible threshold values, which will allow for quick detection. This is the lower boundary.
5) Finally, the threshold value for a detection block has to be selected between the upper and lower boundary.

The example of transients presenting a described method for determining thresholds from simulation tests is shown in Fig. 5a for no-damage operation and in Fig. 5b for operation with a gain error. Based on the presented transients, the speed error threshold can be set as $\lambda_\omega = 0.07$ and the current error threshold can be set as $\lambda_{iq} = 0.01$.

The block diagram of the control structure with a fault simulation and detection block is presented in Fig. 6. The fault simulation module allows for the incorporation of three different failure types: complete signal loss, gain error, and measurement noise. If the position measurement is correct, the value from the encoder will be used. If any type of failure occurs, it will be detected by the detection block described below. In that case, the speed and position of the motor shaft are obtained from the SMO proposed in Section II.

IV. SIMULATION RESULTS

The simulations were conducted within the MATLAB/Simulink environment using a sampling time of 50 μs. The parameters of the surface-mounted PMSM used in the simulations and experiments are shown in Table 1. The simulation results show sensorless operation with and without motor load. The load torque for all presented cases was applied in $t = 0.2$ s and disabled in 0.25 s. Following values were set for detection block: $\gamma_{iq} = 0.2$ A and $\gamma_\omega = 10$ rad/s. The failure in each case was switched on at $t = 0.15$ s.

TABLE 1. Parameters of the machine used in simulation and experiments.

Symbol	Quantity	Value
P_n [W]	nominal power	500
p [-]	pole pairs	5
T_n [Nm]	nominal torque	1.13
I_n [A]	nominal current	12.9
n_n [rpm]	nominal speed	3000
R_s [Ω]	stator resistance	0.258
L_s [mH]	stator inductance	0.6
k_t [Nm/A]	torque constant	0.101
k_e [V/krpm]	back-EMF constant	6.12

Fig. 7 shows the results of the worst failure which is a complete loss of the measuring signal. The detection time in this case is extremely important, because this type of failure may result in a complete loss of stability. At the same time, it is the simplest type of failure to detect, the speed error increases greatly.

Fig. 8 shows the transients of significant state variables during a gain error failure. In the case of such faults, the detection time is extended, but the system operates stably with the highest quality of control. The detection proceeds in

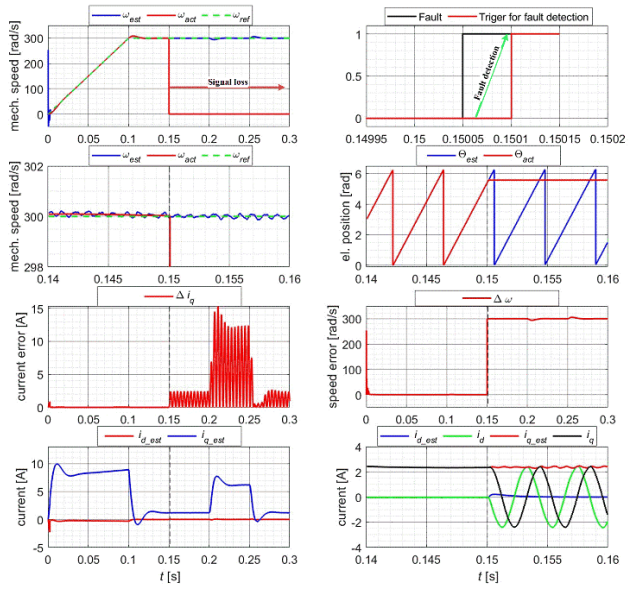

FIGURE 7. Simulation of transients of speed, currents and detector response during the signal loss at $t = 0.15$ s.

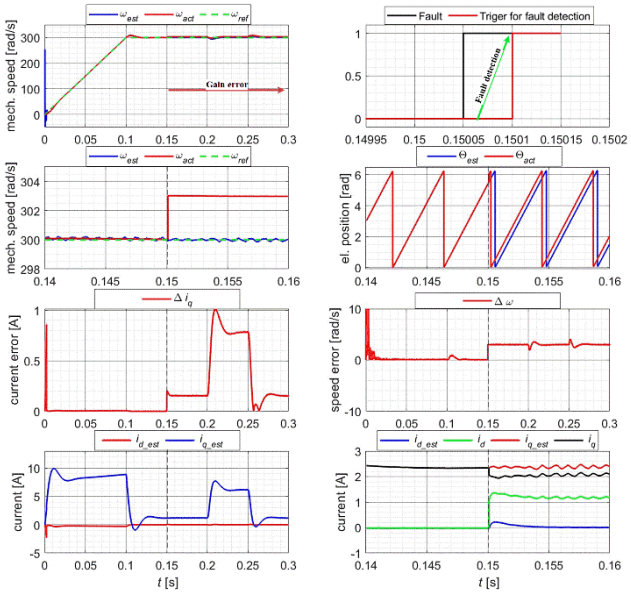

FIGURE 8. Simulation of transients of speed, currents, and detector response during the gain error: +0.5 electrical radians to the measured position and +3 rad/s to the measured speed at $t = 0.15$ s.

the next sample from the occurrence of the fault. In the case of this failure type, the importance of using the current in the q axis in error detection can also be observed.

Fig. 9 shows the transients during measurement noises. The detection time for this type of failure is longer than for a loss of the signal and gain error. However, this is not a failure that significantly worsens the operating properties of the drive system. Comparing the speed and position waveforms, in the case of a signal noise of the tested value, the effect is almost imperceptible.

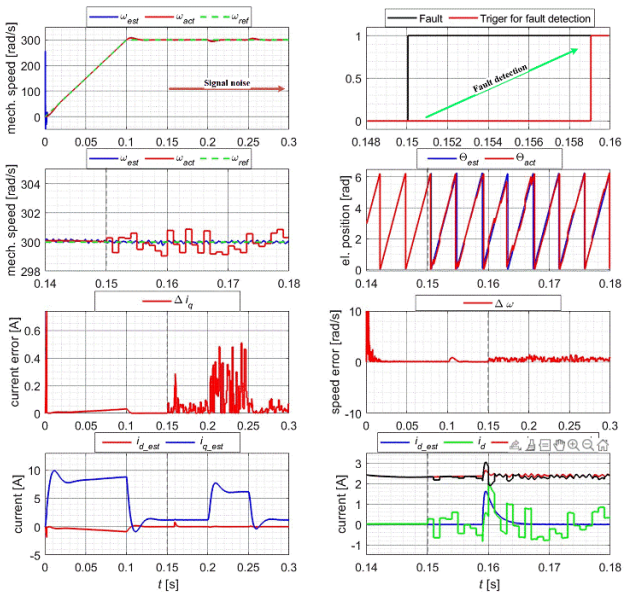

FIGURE 9. Simulation of transients of speed, currents, and detector response during random noise: peaks ±0.4 electrical radians for the position and ±3 rad/s for the speed at $t = 0.15$ s.

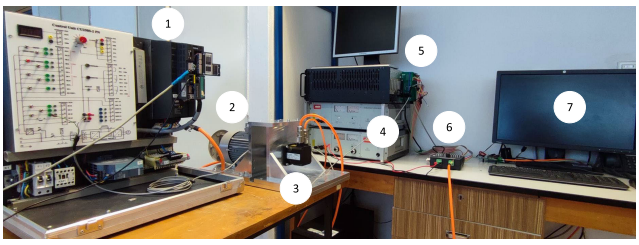

FIGURE 10. Experimental setup: (1) Siemens frequency converter for the control of the load drive, (2) 3kW load induction motor, (3) PMSM for experimental verification, (4) DC power supply, (5) OP5600 HIL Box from OPAL-RT, (6) VSI prototype, (7) Console PC with RT-LAB software.

V. EXPERIMENTAL RESULTS

Experimental tests were performed on the motor with the parameters in Table 1. The OP 5600 HIL Box with RT LAB software from OPAL-RT was used as a real-time controller. The operating parameters of the control algorithm are presented in Table 2. The tested motor was supplied by the VSI prototype, which consists of an integrated power IC IRAM136-3023B with 30 A rated current and 150 V maximum DC voltage. The DC link voltage for the motor used was 48 V. The CKSR 15-NP-LEM were used as current sensors while the actual position was measured by a resolver. The resolver signals were then converted into incremental signals by the electronic prototype device. The final output resolution of the position sensor was 1024 lines per one mechanical revolution. A 3kW induction motor controlled by a Siemens frequency converter was used as a load machine. The test stand with a description of individual elements is shown in Fig. 10.

In experimental conditions, a successful detection was proven for signal loss, gain error and measurement noise. The drive system operated both with the loaded motor and

TABLE 2. Parameters of the control algorithm.

current loop sampling	20 kHz (50 μs)
SMO and fault detector sampling	20 kHz (50 μs)
speed loop sampling	2 kHz (0.5 ms)
PWM frequency	10 kHz (double sampling))
PI current controller	$K_P = 0.12, K_I = 96$
PI speed controller	$K_P = 0.40, K_I = 10$
PLL parameters	$K_P = 1400, K_I = 4{,}9 \cdot 10^5$
shaping coefficient (eq. 7)	$m = 0.012$
feedback gain value (eq. 7)	$k_1 = 100$
cutoff frequency of LPF (eq. 9)	$f_c = 500$ Hz

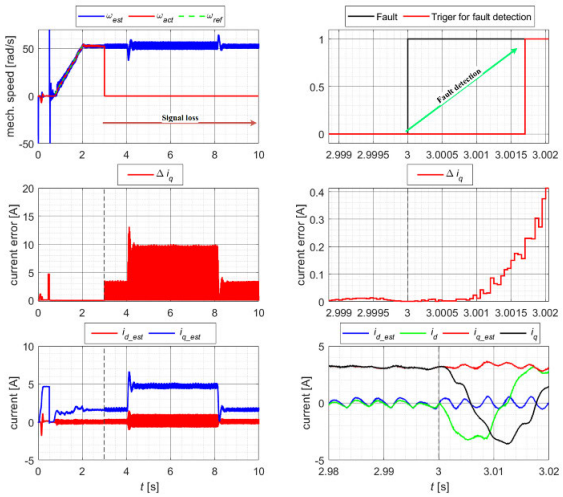

FIGURE 11. Experimental results, transients of speed, rotor angle, currents, and detector response during signal loss for $\omega_{ref} = 50$ rad/s.

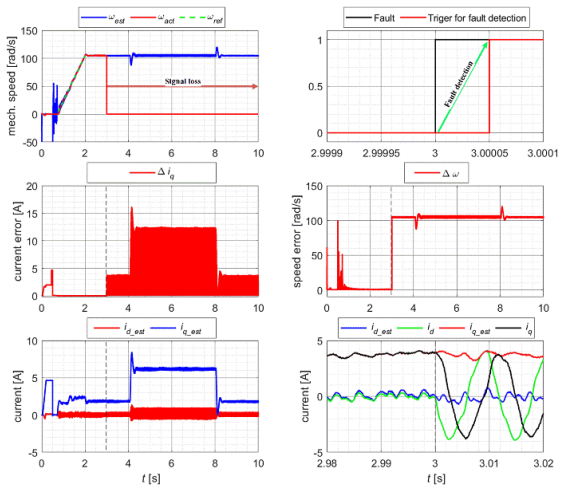

FIGURE 12. Experimental results, transients of speed, rotor angle, currents, and detector response during signal loss for $\omega_{ref} = 100$ rad/s.

without the load. In each case, the load was applied at $t = 4$ s and removed at $t = 8$ s. The system does not lose its stability despite changing operating conditions. Detection threshold γ_{iq} was set to 0.2 A and γ_ω was set to 10 rad/s during the experiments. The experimental tests were also carried out for different speed setpoint values to obtain average detection

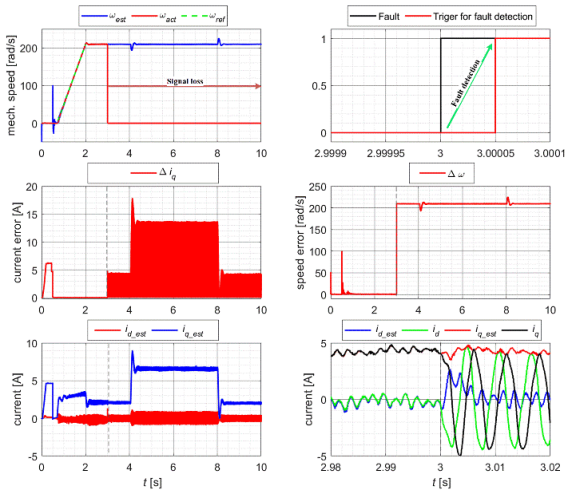

FIGURE 13. Experimental results, transients of speed, rotor angle, currents, and detector response during signal loss for $\omega_{ref} = 200$ rad/s.

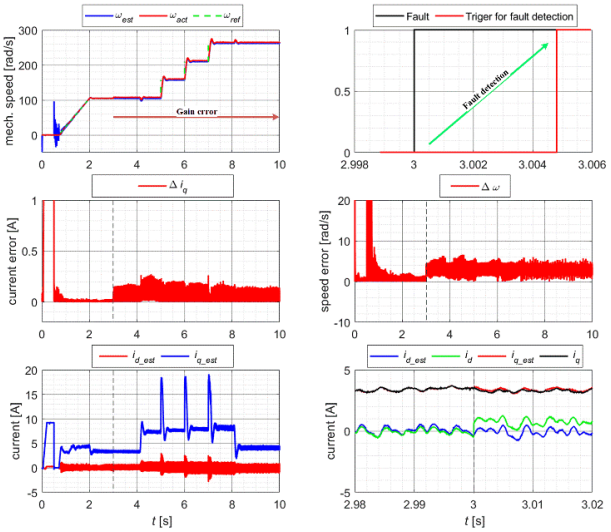

FIGURE 14. Experimental results, transients of speed, currents, and detector response during added offset gain error at $t = 3$ s for added 0.3 rad to electrical angle and 3 rad/s to mechanical speed.

times. The short detection time of the proposed solution made it possible to conduct research over such a wide range of operating parameters. The marking of failure activation represented by the dotted lines and its detection are indicated for all experimental results in this section.

Experimental results for the loss of measuring signal are shown in Fig. 11, Fig. 12 and Fig. 13. The failure was detected in most cases in the first sample after its occurrence. For the lack of the measuring signal, the transients of the rotor angle and speed at the moment of switching to sensorless control are also displayed.

The efficiency of the damage detector at the occurrence of the gain error was checked for 3 different speed values and 2 error values: +0.3 rad and +1 rad added to the measured position. In addition, an offset error of 3 rad/s has been added to the mechanical speed. Example results of the

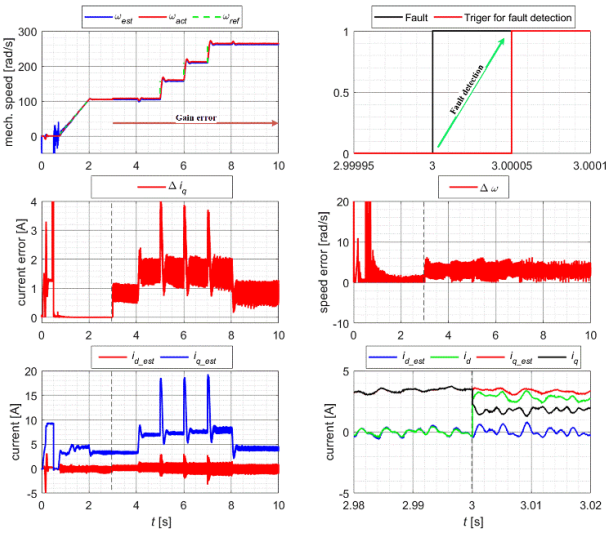

FIGURE 15. Experimental results, transients of speed, currents, and detector response during added offset gain error at $t = 3$ s for added 1 rad to electrical angle and 3 rad/s to mechanical speed.

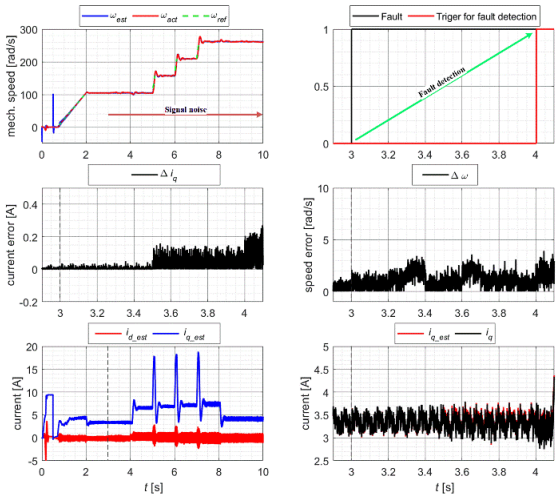

FIGURE 16. Experimental results, transients of speed, currents, and detector response during added random noise at $t = 3$ s for added noise with maximal amplitude of 0.3 rad.

speed, currents, and detector responses are shown in Fig. 14 and Fig. 15.

Detection of the last considered type of fault, measurement noises, was also checked for 3 speed values and for a random noise with 3 maximum amplitude values: 0.1 rad, 0.3 rad and 0.5 rad. Sample results are shown in Fig. 16, Fig. 17 and Fig. 18. In the case of this failure type, the time for its detection is the longest. However, the system does not lose stability when this type of fault is switched on. The speed error increases gradually. Despite the fact that the detection time takes longer here, the system is protected against unexpected performance.

The presented results confirm the detector's efficiency, fast operation time, and the possibility of its application in the FTC system. After switching to the sensorless mode, the system continues to operate with properties similar with the

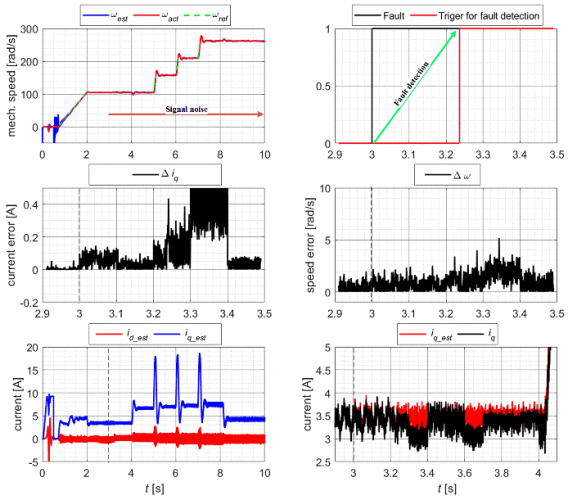

FIGURE 17. Experimental results, transients of speed, currents, and detector response during added random noise at $t = 3$ s for added noise with maximal amplitude of 0.5 rad.

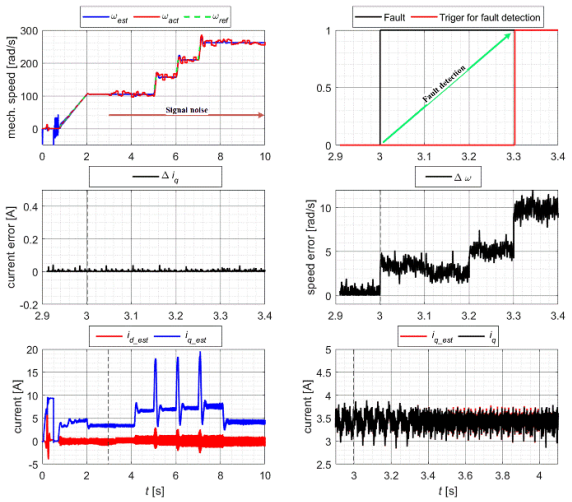

FIGURE 18. Experimental results, transients of speed, currents, and detector response during added random noise at $t = 3$ s for added noise with maximal amplitude of 0.1 rad.

TABLE 3. Average detection time values in [ms] under different operating conditions.

Fault type	Speed setpoint in [rad/s]		
	100	200	260
signal loss	0.05	0.05	0.05
gain error +0.3 rad	5	1.1	0.05
gain error +0.1 rad	0.05	0.05	0.05
noise with max. amplitude ±0.1 rad	300	1000	300
noise with max. amplitude ±0.3 rad	1000	650	550
noise with max. amplitude ±0.5 rad	250	10	2

speed sensor control. A summary of the mean detection times Δt for different speed values is presented in Table 3.

The fastest detection takes place in the case a signal loss. This is a fault that requires immediate detection as it could potentially result in a loss of control stability

with bad consequences. The other faults allow the drive system to operate but could gradually compromise control characteristics. The detection time for these faults increases as the values of gain or noise error become smaller.

VI. CONCLUSION

This article presents a speed sensor fault detection system for the PMSM drive control. The proposed solution is based on the comparison of measured and estimated values of mechanical speed and q-axis current and the estimations are provided via sliding mode observer. The proposed algorithm achieves very short detection times what enables to conduct various experimental tests at a wide range of speeds. The simulation and experimental results are compatible and confirm the effectiveness of the proposed solution and its possibilities in the FTC system. The most important advantages of the solution include:

- short detection time, enabling experimental research,
- very simple algorithm,
- detection of various types of failures, even with a slight influence on the control structure,
- both detection and failure compensation are provided within one algorithm only,
- effective detection under various operating conditions.

Further research will focus on expanding the universality of the detection system. The transition to per-unit variables applied to detector inputs could potentially allow for the development of a detection system suitable for machines with different nominal powers. Additionally, other types of speed observers can be utilized with proposed detector. Therefore, it is necessary to compare the results achieved with other observers to those obtained with the proposed observer.

REFERENCES

[1] Q. Shen, C. Yue, C. H. Goh, and D. Wang, "Active fault-tolerant control system design for spacecraft attitude maneuvers with actuator saturation and faults," *IEEE Trans. Ind. Electron.*, vol. 66, no. 5, pp. 3763–3772, May 2019.

[2] Z. Li, B. Dahhou, Q. Li, and M. Zhang, "Design of passive fault tolerant control of a process system," in *Proc. 27th Chin. Control Decis. Conf. (CCDC)*, Qingdao, China, May 2015, pp. 2776–2781.

[3] J. Zhang, Z. Pang, Y. Zhou, and C. Han, "Active fault tolerant control for networked control systems with actuator fault," in *Proc. 35th Chin. Control Conf. (CCC)*, Chengdu, China, Jul. 2016, pp. 7521–7525.

[4] A. Najafi, M. T. Vu, S. Mobayen, J. H. Asad, and A. Fekih, "Adaptive barrier fast terminal sliding mode actuator fault tolerant control approach for quadrotor UAVs," *Mathematics*, vol. 10, no. 16, p. 3009, Aug. 2022.

[5] K. Naseri, M. T. Vu, S. Mobayen, A. Najafi, and A. Fekih, "Design of linear matrix inequality-based adaptive barrier global sliding mode fault tolerant control for uncertain systems with faulty actuators," *Mathematics*, vol. 10, no. 13, p. 2159, Jun. 2022.

[6] C. Wu, C. Guo, Z. Xie, F. Ni, and H. Liu, "A signal-based fault detection and tolerance control method of current sensor for PMSM drive," *IEEE Trans. Ind. Electron.*, vol. 65, no. 12, pp. 9646–9657, Dec. 2018.

[7] H. T. Canseven and A. Ünsal, "Performance improvement of fault-tolerant control for dual three-phase PMSM drives under inter-turn short circuit faults," in *Proc. 47th Annu. Conf. IEEE Ind. Electron. Soc. (IECON)*, Toronto, ON, Canada, Oct. 2021, pp. 1–5.

[8] A. Akrad, M. Hilairet, and D. Diallo, "Design of a fault-tolerant controller based on observers for a PMSM drive," *IEEE Trans. Ind. Electron.*, vol. 58, no. 4, pp. 1416–1427, Apr. 2011.

[9] A. Bellini, F. Filippetti, C. Tassoni, and G.-A. Capolino, "Advances in diagnostic techniques for induction machines," *IEEE Trans. Ind. Electron.*, vol. 55, no. 12, pp. 4109–4126, Dec. 2008.

[10] G. Zhang, G. Wang, G. Wang, J. Huo, L. Zhu, and D. Xu, "Fault diagnosis method of current sensor for permanent magnet synchronous motor drives," in *Proc. Int. Power Electron. Conf. (IPEC-Niigata -ECCE Asia)*, Niigata, Japan, May 2018, pp. 1206–1211.

[11] M. Bouakoura, N. Nait-Said, and M.-S. Nait-Said, "Speed sensor fault diagnosis in an induction motor vector controlled drive," *Acta Electrotech. Inf.*, vol. 17, no. 1, pp. 49–57, 2017.

[12] I. Jlassi and A. J. M. Cardoso, "A single fault diagnostics approach for power switches, speed sensors and current sensors in regenerative PMSM drives," in *Proc. IEEE 11th Int. Symp. Diag. for Electr. Mach., Power Electron. Drives (SDEMPED)*, Tinos, Greece, Aug. 2017, pp. 366–372.

[13] S. K. Kommuri, S. B. Lee, and K. C. Veluvolu, "Robust sensors-fault-tolerance with sliding mode estimation and control for PMSM drives," *IEEE/ASME Trans. Mechatronics*, vol. 23, no. 1, pp. 17–28, Feb. 2018.

[14] Z. Makhataeva, B. Sarsembayev, and T. D. Do, "Fault-tolerant control of IPMSMs based on an modified sliding mode observer," in *Proc. Int. Conf. Syst. Sci. Eng. (ICSSE)*, Dong Hoi, Vietnam, Jul. 2019, pp. 526–530.

[15] Y. Bensalem, A. Kouzou, R. Abbassi, H. Jerbi, R. Kennel, and M. Abdelrahem, "Sliding-mode-based current and speed sensors fault diagnosis for five-phase PMSM," *Energies*, vol. 15, no. 1, p. 71, Dec. 2021.

[16] M. Bourogaoui, I. Jlassi, S. K. E. Khil, and H. B. A. Sethom, "An effective encoder fault detection in PMSM drives at different speed ranges," in *Proc. IEEE 10th Int. Symp. Diag. Electr. Mach., Power Electron. Drives (SDEMPED)*, Guarda, Portugal, Sep. 2015, pp. 90–96.

[17] P. F. Odgaard and J. Stoustrup, "Unknown input observer based detection of sensor faults in a wind turbine," in *Proc. IEEE Int. Conf. Control Appl.*, Yokohama, Japan, Sep. 2010, pp. 310–315.

[18] M. H. Salem, Y. Bensalem, and M. N. Abdelkrim, "A speed sensor fault tolerant control for a permanent magnet synchronous motor," in *Proc. 17th Int. Multi-Conf. Syst., Signals Devices (SSD)*, Monastir, Tunisia, Jul. 2020, pp. 290–295.

[19] H. Zhao, P. Luo, N. Wang, Z. Zheng, and Y. Wang, "Fuzzy logic control of the fault-tolerant PMSM servo system based on MRAS observer," in *Proc. Chin. Control Decis. Conf. (CCDC)*, Shenyang, China, Jun. 2018, pp. 1812–1817.

[20] G. F. H. Beng, X. Zhang, and D. M. Vilathgamuwa, "Sensor fault-resilient control of interior permanent-magnet synchronous motor drives," *IEEE/ASME Trans. Mechatronics*, vol. 20, no. 2, pp. 855–864, Apr. 2015.

[21] Q. Zhu, Z. Li, X. Tan, D. Xie, and W. Dai, "Sensors fault diagnosis and active fault-tolerant control for PMSM drive systems based on a composite sliding mode observer," *Energies*, vol. 12, no. 9, p. 1695, May 2019.

[22] V. Utkin, J. Guldner, and J. Shi, *Sliding Mode Control in Electromechanical Systems*, 1st ed. London, U.K.: Taylor & Francis, 1999.

[23] C. Gong, Y. Hu, J. Gao, Y. Wang, and L. Yan, "An improved delay-suppressed sliding-mode observer for sensorless vector-controlled PMSM," *IEEE Trans. Ind. Electron.*, vol. 67, no. 7, pp. 5913–5923, Jul. 2020.

[24] S. Ye and X. Yao, "An enhanced SMO-based permanent-magnet synchronous machine sensorless drive scheme with current measurement error compensation," *IEEE J. Emerg. Sel. Topics Power Electron.*, vol. 9, no. 4, pp. 4407–4419, Aug. 2021.

[25] K. Kyslan, V. Petro, P. Bober, V. Šlapák, F. Ďurovský, M. Dybkowski, and M. Hric, "A comparative study and optimization of switching functions for sliding-mode observer in sensorless control of PMSM," *Energies*, vol. 15, no. 7, p. 2689, Apr. 2022.

[26] S. M. Kazraji, R. B. Soflayi, and M. B. B. Sharifian, "Sliding-mode observer for speed and position sensorless control of linear-PMSM," *Electr., Control Commun. Eng.*, vol. 5, no. 1, pp. 20–26, May 2014.

[27] G. Wang, G. Zhang, and D. Xu, *Position Sensorless Control Techniques for Permanent Magnet Synchronous Machine Drives*, 1st ed. Singapore: Springer, 2020.

[28] L. Harnefors and H.-P. Nee, "A general algorithm for speed and position estimation of AC motors," *IEEE Trans. Ind. Electron.*, vol. 47, no. 1, pp. 77–83, Feb. 2000.

[29] G. Wang, Z. Li, G. Zhang, Y. Yu, and D. Xu, "Quadrature PLL-based high-order sliding-mode observer for IPMSM sensorless control with online MTPA control strategy," *IEEE Trans. Energy Convers.*, vol. 28, no. 1, pp. 214–224, Mar. 2013.

[30] G. Wang, L. Ding, Z. Li, J. Xu, G. Zhang, H. Zhan, R. Ni, and D. Xu, "Enhanced position observer using second-order generalized integrator for sensorless interior permanent magnet synchronous motor drives," *IEEE Trans. Energy Convers.*, vol. 29, no. 2, pp. 486–495, Jun. 2014.

[31] S. Chi, Z. Zhang, and L. Xu, "Sliding-mode sensorless control of direct-drive PM synchronous motors for washing machine applications," *IEEE Trans. Ind. Appl.*, vol. 45, no. 2, pp. 582–590, Mar./Apr. 2009.

KAMILA JANKOWSKA received the M.Sc. degree in electrical engineering from the Faculty of Electrical Engineering, Wrocław University of Science and Technology, Wrocław, Poland, in 2020, where she is currently pursuing the Ph.D. degree in sensor fault tolerant control systems with PMSM with the Department of Electrical Machines, Drives and Measurement. Her main interests include fault-tolerant control systems based on artificial intelligence methods and analytical compensation.

VIKTOR PETRO was born in Košice, Slovakia. He received the M.Sc. and Ph.D. degrees in electrical engineering from the Faculty of Electrical Engineering and Informatics, Technical University of Košice, Slovakia, in 2020 and 2023, respectively. He is currently a Software Developer. His research interest includes position-sensorless control for permanent magnet synchronous motors, focusing on sliding-mode and signal injection-based control approaches.

MATEUSZ DYBKOWSKI received the M.Sc., Ph.D., and D.Sc. degrees from the Faculty of Electrical Engineering, Wrocław University of Technology, Wrocław, Poland, in 2004, 2008, and 2014, respectively. Since 2008, he has been a member of the academic staff with the Division of Electrical Drives Control, Department of Electrical Machines, Drives and Measurements, Wrocław University of Technology. He is the author or coauthor of more than 150 publications, one thesis, one monograph, 14 chapters in monographs, and more than 78 scientific papers in refereed conference proceedings and journals. His research interests include induction-motor drive control and state-variable estimations, control-theory applications in electrical drives, ac generators, digital-signal processors, and field-programmable gate array applications.

KAROL KYSLAN (Member, IEEE) received the M.Sc. and Ph.D. degrees in electrical engineering and the Habilitation degree from the Technical University of Košice, Slovakia, in 2009, 2012, and 2020, respectively. He is currently an Associate Professor with the Department of Electrical Engineering and Mechatronics and the Vice-Dean of the Faculty of Electrical Engineering and Informatics, Technical University of Košice. He has published more than 40 scientific papers in refereed conference proceedings and journals and holds one national patent. His research interests include the control of electrical drives and motion control, finite control set model predictive control, sensorless control, and dynamic load emulation.